

# Account of baryonic feedback effect in the $\gamma$ -ray measurements of intergalactic magnetic fields

Kyrylo Bondarenko<sup>1, 2</sup>, Alexey Boyarsky<sup>3</sup>, Alexander Korochkin<sup>4, 5, 6</sup>,  
Andrii Neronov<sup>4, 7</sup>, Dmitri Semikoz<sup>4, 5, 8</sup>, Anastasia Sokolenko<sup>9</sup>

<sup>1</sup> Theoretical Physics Department, CERN, Geneva 23, CH-1211, Switzerland

<sup>2</sup> L'Ecole polytechnique federale de Lausanne, 1015 Lausanne, Switzerland

<sup>3</sup> Institute Lorentz, Leiden University, Niels Bohrweg 2, Leiden, NL-2333 CA, the Netherlands

<sup>4</sup> APC, Universite Paris Diderot, CNRS/IN2P3, CEA/IRFU e-mail: alexander.korochkin@apc.in2p3.fr

<sup>5</sup> Institute for Nuclear Research of the Russian Academy of Sciences, 60th October Anniversary st. 7a, 117312, Moscow, Russia

<sup>6</sup> Novosibirsk State University, Pirogova 2, Novosibirsk, 630090 Russia

<sup>7</sup> Astronomy Department, University of Geneva, Ch. d'Ecogia 16, 1290, Versoix, Switzerland

<sup>8</sup> National Research Nuclear University MEPhI, 115409 Moscow, Russia

<sup>9</sup> Institute of High Energy Physics, Austrian Academy of Sciences, Nikolsdorfergasse 18, 1050 Vienna, Austria

June 8, 2021

## ABSTRACT

Intergalactic magnetic fields in the voids of the large-scale structure can be probed via measurements of secondary  $\gamma$ -ray emission from  $\gamma$ -ray interactions with extragalactic background light. Lower bounds on the magnetic field in the voids were derived from the non-detection of this emission. It is not clear a-priori what kind of magnetic field is responsible for the suppression of the secondary  $\gamma$ -ray flux: a cosmological magnetic field that might be filling the voids or the field spread by galactic winds driven by star formation and active galactic nuclei. Here we use IllustrisTNG cosmological simulations to study the influence of magnetized galactic wind bubbles on the secondary  $\gamma$ -ray flux. We show that within the IllustrisTNG model of baryonic feedback, the galactic wind bubbles typically provide energy-independent secondary flux suppression at the level of about 10%. The observed flux suppression effect has to be due to the cosmological magnetic field in the voids. This might not be the case for a special case when the primary  $\gamma$ -ray source has a hard intrinsic  $\gamma$ -ray spectrum peaking in the energy range above 50 TeV. In this case, the observational data may be strongly affected by the magnetized bubble blown by the source host galaxy.

## 1. Introduction

Magnetic fields in galaxies and clusters are believed to result from amplification of initial seeds fields that might be of primordial origin (see e.g. [Durrer & Neronov \(2013\)](#) for a review). This possibility suggests that measurement of parameters of the seed fields can provide a new cosmological observable, a new “window” on the Early Universe, more specifically on the epochs pre-dating the epoch of formation of the Cosmic Microwave Background signal. Large-scale magnetic fields that fill the volume of the voids of the Large Scale Structure (LSS) likely did not experience adiabatic contraction or dynamo amplification that transformed the seed fields in galaxies and galaxy clusters. The properties of these volume-filling intergalactic magnetic fields (IGMF) might therefore be close to the properties of the cosmological seed fields.

The technique of measurements of IGMF best suited for probing magnetic fields in the voids is based on  $\gamma$ -ray observations of distant active galactic nuclei (AGN). The technique exploits the effect of attenuation of very-high-energy (VHE)  $\gamma$ -ray flux from distant AGN by the effect of pair production on photons of Extragalactic Background Light (EBL). This leads to the development of an electromagnetic cascade along the line of sight. The cascade emission is observable in the form of magnetic field dependent delayed ([Plaga 1995](#)) or extended ([Neronov & Semikoz 2007, 2009](#)) emission around the primary AGN point source. Searches for extended and delayed  $\gamma$ -ray emission in the energy band of Fermi Large Area Telescope (LAT) has not

yielded measurements of the void IGMF but have imposed a lower bound on its strength ([Neronov & Vovk 2010](#); [Taylor et al. 2011](#); [Dermer et al. 2011](#)). The most recent analysis of Fermi/LAT data reported by [Ackermann et al. \(2018\)](#) constrains the IGMF in the voids to be stronger than  $\sim 10^{-16}$  G for large correlation length magnetic fields and  $\sim 10^{-14}$  G for short correlation length field originating from the Early Universe. Next-generation  $\gamma$ -ray telescope CTA will be able to probe stronger IGMF with strength up to  $\sim 10^{-12}$  G ([Korochkin et al. 2021](#); [Abdalla et al. 2021](#)).

Even if CTA will succeed to measure the IGMF strength in the voids of the LSS, it is not clear a-priori if this field can be identified as the primordial field. The problem is that the voids can be “polluted” by the magnetic field spread by the baryonic feedback process that returns matter from galaxies into the intergalactic medium. The galactic winds driven by the supernova and AGN activity are most probably ionized and carry magnetic fields with them ([Bertone et al. 2006](#); [Pinsonneault et al. 2010](#)). Uncertainties of the details of the baryonic feedback on the LSS do not allow to answer the question if the magnetic field spread by the feedback can fill the voids and thus hide the primordial field. If this is the case, measurement of IGMF with CTA will fail to provide a new cosmological observable. Instead, it would rather provide constraints on the baryonic feedback process.

The magnetized galactic winds can affect the  $\gamma$ -ray measurements of IGMF only if they produce IGMF with volume filling factor of the order of unity ([Dolag et al. 2011](#)). Indeed, the mean free path of  $\gamma$ -rays with energies in the 10-30 TeV range is in

the 0.1-1 Gpc range. The extended and delayed emission from electrons and positrons deposited in the intergalactic medium by the pair production process is accumulated all over this length scale. The extended and delayed  $\gamma$ -ray signal is sensitive to the field that spans the largest part of the line of sight toward distant AGN. If the baryonic feedback field is concentrated in the nodes and filaments of the LSS, the delayed and extended  $\gamma$ -ray signal is not strongly affected by the feedback field and  $\gamma$ -ray measurements can still provide information on the primordial field.

Significant progress toward better modeling of the baryonic feedback process has been recently achieved by IllustrisTNG cosmological simulations (Nelson et al. 2018; Springel et al. 2018; Pillepich et al. 2018a; Naiman et al. 2018; Marinacci et al. 2018). Recently, Garcia et al. (2020) have used IllustrisTNG to show that AGN and supernovae driven outflows create extended magnetized bubbles with magnetic fields of the order of  $B > 10^{-12}$  G and typical sizes in the range of  $\sim 10 - 30$  Mpc with magnetic field with parameters largely independent from those of the pre-existing seed magnetic fields.

In what follows, we use the IllustrisTNG model to assess the effect of contamination of the intergalactic medium by magnetic field spread by the galactic winds and its consequences for the measurements of primordial IGMF. We consider several characteristics situations of VHE  $\gamma$ -ray sources at different distances, with different  $\gamma$ -ray spectra, situated inside and outside the galactic wind bubbles. We find that within the IllustrisTNG baryonic feedback model, the basic features of the extended or delayed  $\gamma$ -ray signal sensitive to the primordial IGMF are just slightly altered, typically by 10-20%. This does not preclude the possibility of measurement of the primordial field in the voids, introducing, however an additional systematic uncertainty to be properly taken into account in the analysis with the future instruments.

## 2. Magnetized bubbles in IllustrisTNG simulations

### 2.1. TNG simulations

IllustrisTNG is a set of gravo-magnetohydrodynamic simulations, the next generation (TNG) of the Illustris project (Nelson et al. 2018; Springel et al. 2018; Pillepich et al. 2018a; Naiman et al. 2018; Marinacci et al. 2018) that is based on the moving-mesh AREPO code (Springel 2010) that solves the system of equations for the self-gravity and ideal magnetohydrodynamic (Pakmor et al. 2011; Pakmor & Springel 2013). Cosmological parameters are chosen to be equal to the best fit Planck 2015 cosmological parameters (Planck Collaboration et al. 2016).

We use the highest resolution simulation that are publicly available TNG100-1 (TNG100) (Nelson et al. 2019b). The TNG100 simulation has a box size  $\sim (110 \text{ cMpc})^3$  and contains  $1820^3$  dark matter particles and an equal number of initial gas cells with masses of  $m_{\text{DM}} = 7.5 \times 10^6 M_{\odot}$  and  $m_{\text{bar}} = 1.4 \times 10^6 M_{\odot}$ .

The initial seed magnetic field in this run is a constant magnetic field with field strength  $10^{-14}$  cG (comoving Gauss) directed along the  $z$  axis in the simulation box. This seed magnetic field experiences adiabatic contraction during the structure formation process, and then it is strongly amplified by small-scale dynamos in collapsed structures.

The TNG simulations adopt a comprehensive galaxy and supermassive black holes (SMBH) formation and feedback model (Weinberger et al. 2017a; Pillepich et al. 2018b). SMBHs with an initial mass of  $\sim 10^6 M_{\odot}$  are placed in the gravitational potential minima of dark matter halos when the virial mass ex-

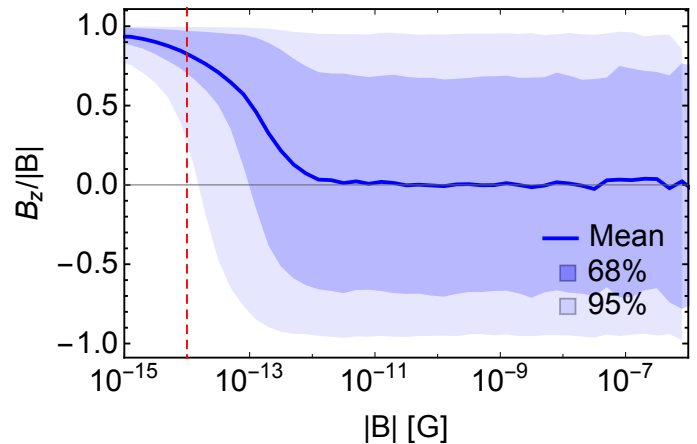


**Fig. 1.** Orientation of the magnetic field along the  $z$  direction as a function of the magnetic field strength at redshift 0. The blue line shows the mean value, while dark and light blue shaded regions represent areas with 68% and 95% of simulation volume. The red dashed line shows the seed magnetic field value  $B = 10^{-14}$  G.

ceeds  $\sim 7 \times 10^{10} M_{\odot}$ . These black holes grow via binary mergers with each other or via smooth gas accretion according to the Bondi-Hoyle-Lyttleton model (Weinberger et al. 2017b). The black hole growth rate depends on the black hole mass, local gas density, and relative velocity between the black hole and its surroundings.

Within the IllustrisTNG model, the SMBH activity has two different regimes that correspond to high-accretion and low-accretion states (Weinberger et al. 2017a). In the high-accretion rate state (accretion rate above  $\sim 10\%$  of the Eddington limit), the energy is continuously injected into the surrounding gas, causing thermal heating of the gas. In the low-accretion rate state, the kinetic energy is deposited periodically, once enough energy accumulates via accretion (see Weinberger et al. 2017a for additional details). Each injection event creates a randomly oriented high-velocity kinetic wind. If averaged over large time intervals, energy injection in this mode also becomes isotropic. It is the low accretion rate feedback mode that drives the most powerful outflows in the TNG model (Nelson et al. 2019a). A large fraction of the injected kinetic energy in this mode thermalizes via shocks in the surrounding gas, thereby providing a distributed heating channel.

### 2.2. Magnetic bubbles

According to the TNG simulations, magnetized bubbles (larger-than-galaxy size regions with magnetic fields over  $10^{-12}$  G, orders of magnitude larger than the initial seed field) of chemically enriched material emerge at  $z \lesssim 2$  as a result of active baryonic feedback from galaxies (Garcia et al. 2020, 2021). These bubbles are significantly non-spherical and can have sizes of the order of tens of Mpc. Garcia et al. (2020) demonstrated that at  $z = 0$  such bubbles occupy 12 – 14% of cosmological volume for magnetic fields stronger than  $10^{-12}$  G and more than 3% for  $B > 10^{-9}$  G. Comparing the simulations with many orders of magnitude different initial magnetic field (otherwise identical), Garcia et al. (2020, 2021) have shown that magnetic fields in the bubbles are to a large extent independent of the strength of the initial seed field. Fig. 1 illustrates this effect: orientation of strong magnetic fields with  $B > 10^{-12}$  cG “forgets” about the direction of the seed field (that was along  $z$ -axes in TNG simulations). In con-

trast, weak fields in the “real” IGM outside bubbles prefer the initial direction. It was also demonstrated in [Garcia et al. \(2020\)](#) that the bubbles are caused mainly by the AGN activity (with a smaller supernova contribution).

### 2.3. Line-of-sight data

We are interested in the effects of the bubbles on the extended and delayed  $\gamma$ -ray signal from distant AGN. To assess these effects, we have extracted from the TNG-100 simulation volume data on the strength and orientation of magnetic field along randomly chosen straight lines, “lines of sight” (LOS), originating from 7 different SMBHs with masses from  $10^8 M_\odot$  to  $10^{10} M_\odot$ . The SMBHs were selected requiring sufficient released energy in the low-accretion rate feedback mode,  $E_{\text{low}} > 10^{58.5}$  erg. Using continuous boundary conditions in the simulation box, we produce four randomly oriented lines of sight with lengths up to 600 Mpc per AGN. Magnetic fields are calculated as average values inside voxels of the size  $(20 \text{ kpc})^3$  using the publicly available pysph-viewer code ([Benitez-Llambay 2015](#)). Examples of two lines of sights starting from AGN within and outside bubbles with strong magnetic field are shown in [Fig. 2](#).

## 3. Numerical modeling

To explore the effects of magnetic bubbles on the secondary emission, we performed numerical modeling of the propagation of the high energy gamma-rays through the cosmic medium using data on a magnetic field for a set of lines of sight extracted from the TNG100 simulation. For this purpose, we use the recently developed Monte Carlo simulation code CRbeam ([Berezinsky & Kalashev 2016](#)) taking into account gamma-ray absorption with pair production on the EBL, subsequent inverse Compton scattering of electrons and positrons on CMB and EBL, and deflection of charged component in magnetic fields. This code was also tested via comparison with several alternative cascade codes ([Taylor et al. 2011](#); [Kalashev & Kido 2015](#); [Kachelriess et al. 2012](#)).

In all simulations position of the source corresponds to the first voxel of the LOS. The directions of the initial momenta of all particles are the same and coincide with the direction along the LOS. The strength and direction of magnetic fields are given by linear interpolation between neighboring voxels. Secondary  $\gamma$ -ray signal generated by every electron and positron depends only on the strength and orientation of the magnetic field right at the location of electron-positron pair production (more precisely within the voxel in which the pair production happens). This appears to be reasonable in the view of the fact that electrons with energies  $E_e < 5$  TeV (which produce secondary gamma-rays with  $E_\gamma < 100$  GeV) are typically deflected by  $\delta > 3^\circ$  already within the first 20 kpc of their trajectory. Since we are interested only in secondary  $\gamma$ -rays emitted within the angle comparable to the point spread function (PSF) of  $\gamma$ -ray telescopes,  $\theta_{psf} \lesssim 1$ , further  $\gamma$ -ray production by electrons/positrons deflected by more than several degrees does not contribute to the secondary  $\gamma$ -ray signal sampled by the telescope situated on the LOS.

In order to separately study the effect of bubbles and voids on the cascade component, we construct for each LOS three alternative magnetic field profiles:

- Only voids: in all voxels where  $B \geq 10^{-12}$  G we set  $B = 0$  G.

- Only bubbles: magnetic field in all voids with  $B < 10^{-12}$  G and in the first bubble around the source AGN are set to  $B = 0$  G.
- Only the AGN source bubble: magnetic fields everywhere outside the first bubble are set to  $B = 0$  G. To avoid the influence of random fluctuations of the magnetic field and make the procedure for determining the size of the first bubble more stable, we define the boundary of the first bubble as the point from which the magnetic field strength is below  $10^{-12}$  G for at least 300 kpc.

We propagate  $\gamma$ -rays from the source to the observer for each magnetic field profile and calculate the secondary  $\gamma$ -ray signal along the LOS. For LOSs containing only the first bubble, potentially more significant fluctuations of the secondary flux may arise due to the fact that all primary photons are emitted in the same direction. In reality, the primary  $\gamma$ -rays are emitted in a cone with an opening angle  $\alpha_{jet}$  so that they sense different directions in the bubble. The bubble properties in various directions are different (size, magnetic field profile). In our analysis, we neglect this difference and believe that the bubble radius changes insignificantly on the scale of the jet opening angle.

We explore several possible spectral models of the AGN source. The intrinsic  $\gamma$ -ray spectrum of the source is always a cutoff power-law  $dN/dE \propto E^{-\Gamma} \exp(-E/E_{cut})$ . The slope of the power-law is  $\Gamma = 1.7$ . To the contrary,  $E_{cut}$  is a free parameter. Another free parameter is the distance to the observer  $D_s$  which sets the redshift of the source  $z$ . We scan over parameter space choosing  $E_{cut}$  in 1-100 TeV range and  $0.025 < z < 0.15$ . Cosmological parameters are set to  $H_0 = 70$  km/(s Mpc),  $\Omega_m = 0.3$  and  $\Omega_\Lambda = 0.7$  and the EBL model is fixed to that of [Gilmore et al. \(2012\)](#).

We propagate  $\gamma$ -rays until they reach the sphere with radius  $r = D_s$ . Despite the fact that all primary particles are emitted in the same direction, we are able to model primary photon emission into a jet with an opening angle  $\alpha_{jet}$  by recording the  $\gamma$ -rays that hit the part of the sphere lying inside the cone with the opening angle  $\alpha_{jet} = 5^\circ$  whose axis coincides with the direction from the source to the observer. For the spectral plots presented in the next section, we retain only the  $\gamma$ -rays that arrive at the position of the telescope at an incidence angle within the telescope PSF, which we assume to be  $\theta_{psf} = 0.3^\circ$ .

## 4. Results

The simulated spectra of the primary AGN source and secondary  $\gamma$ -ray emission are shown in [Figures 3, 4 and 5](#). They represent three types of magnetic field profiles and four different choices of parameters of the AGN source: a nearby source with low energy cut-off, a nearby source with high energy cut-off, a distant source with low energy cut-off, and a distant source with high energy cut-off.

The three sets of figures show that the effect of the void IGMF on the secondary  $\gamma$ -ray signal ([Fig. 3](#)) is clearly different from the effect of the bubble magnetic fields ([Figs. 4 and 5](#)).

The volume-filling IGMF outside bubbles produces complete suppression of the secondary  $\gamma$ -ray emission at  $E < 100$  GeV. As the initial conditions of TNG100 contain a constant magnetic field with the strength  $B = 10^{-14}$  G, this part of IGMF, unaffected by galactic dynamos, has large correlation length and  $B > 10^{-15}$  G almost everywhere (see [Fig. 2](#) in [Garcia et al. \(2020\)](#)). Therefore, such an effect on the secondary  $\gamma$ -ray emission is not unexpected, based on the analytical estimates of ([Neronov & Semikoz 2007, 2009](#)).

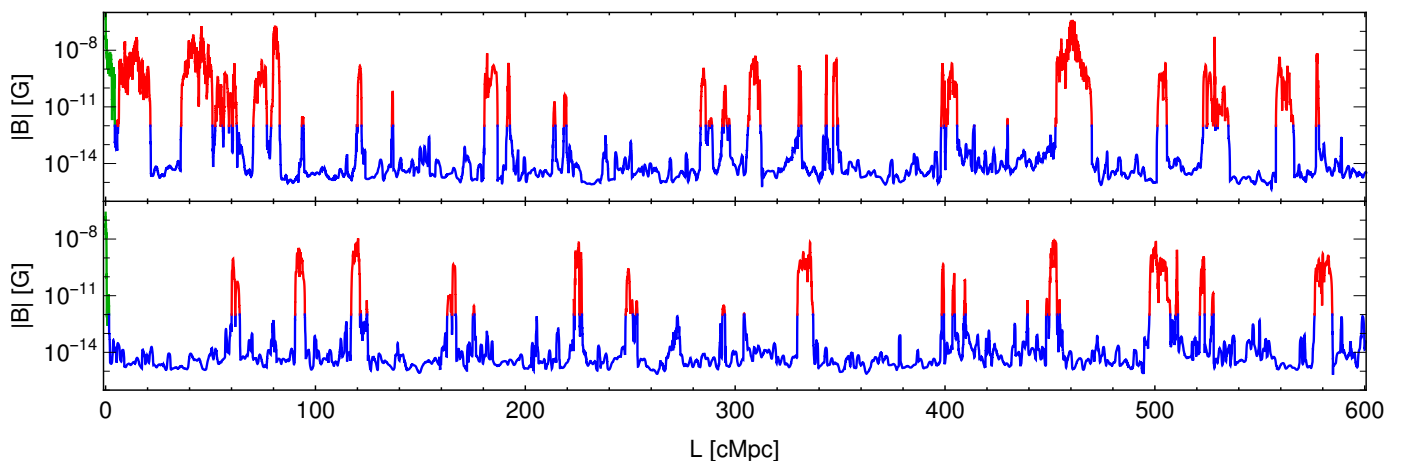


**Fig. 2.** Examples of magnetic field profiles along two 600 Mpc long LOS that start at AGN found in the TNG-100 simulation. The upper panel shows LOS starting inside a strong magnetic field bubble at the beginning correspond to the AGN-3. The lower panel shows an example of the LOS starting from AGN-2 within a small bubble. We indicated the first bubble with green color, other bubbles with red, and voids with blue. See details of this division in section 3.

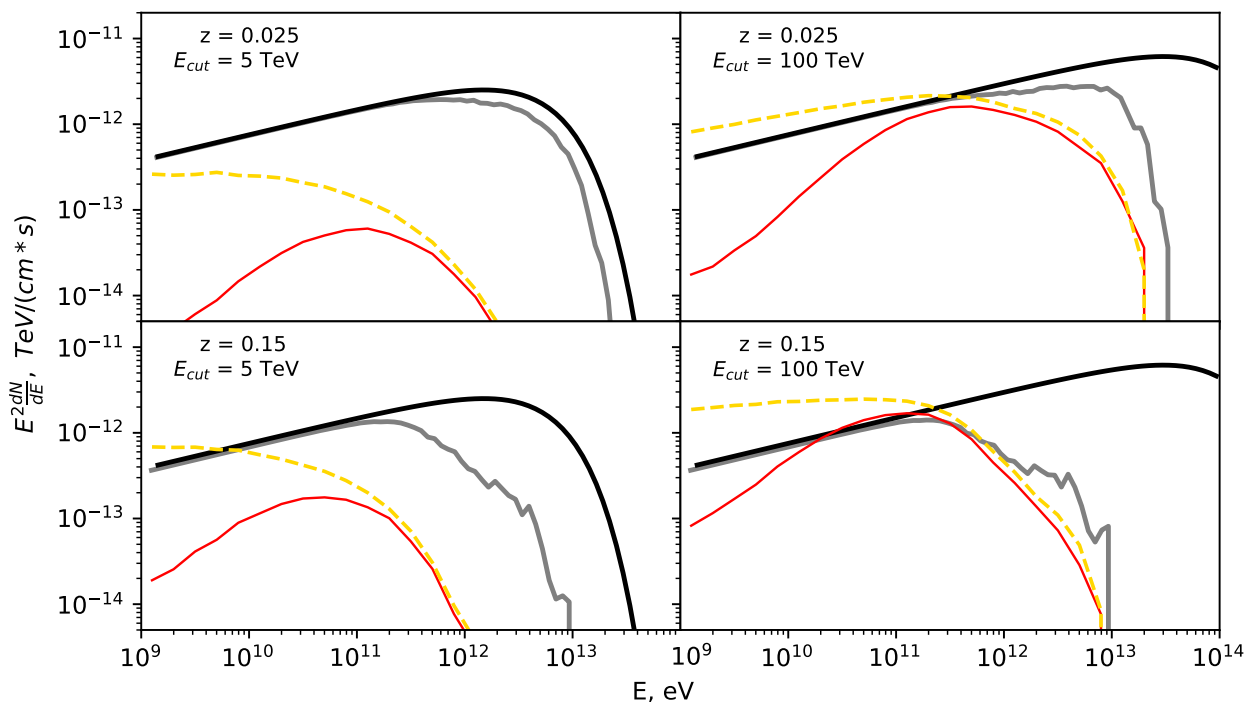


**Fig. 3.** Primary and secondary  $\gamma$ -ray spectra for the “only voids” magnetic field profile (only regions with  $B \leq 10^{-12}$  G are taken into account). Different subplots represent different parameters of the source. Black and gray solid lines are the intrinsic and observed primary source spectra. Yellow dashed lines show the secondary  $\gamma$ -ray flux for zero LOS magnetic field. Red solid lines show the secondary  $\gamma$ -ray flux with a nonzero magnetic field in the voids.

The magnetized bubbles produce a qualitatively different effect on the secondary  $\gamma$ -ray flux. Strong ( $B > 10^{-12}$  G) magnetic fields in the bubbles sufficiently deflect charged particles created in the bubbles and therefore completely suppress their secondary  $\gamma$ -ray flux at the detector all across its energy range. This changes the overall normalization of the secondary emission, but influences only very little its shape.

This qualitative difference between the effects of void IGMF and bubbles holds for the whole range of properties of the primary  $\gamma$ -ray sources. Only the strength of the overall flux suppression by the bubbles depends on the source parameters.

The level of secondary flux suppression depends, of course, on the length of the bubbles along the line of sight from the sources towards the observer. Fig. 6 shows lost secondary flux in percentage points for all the simulated lines of sight. One can see

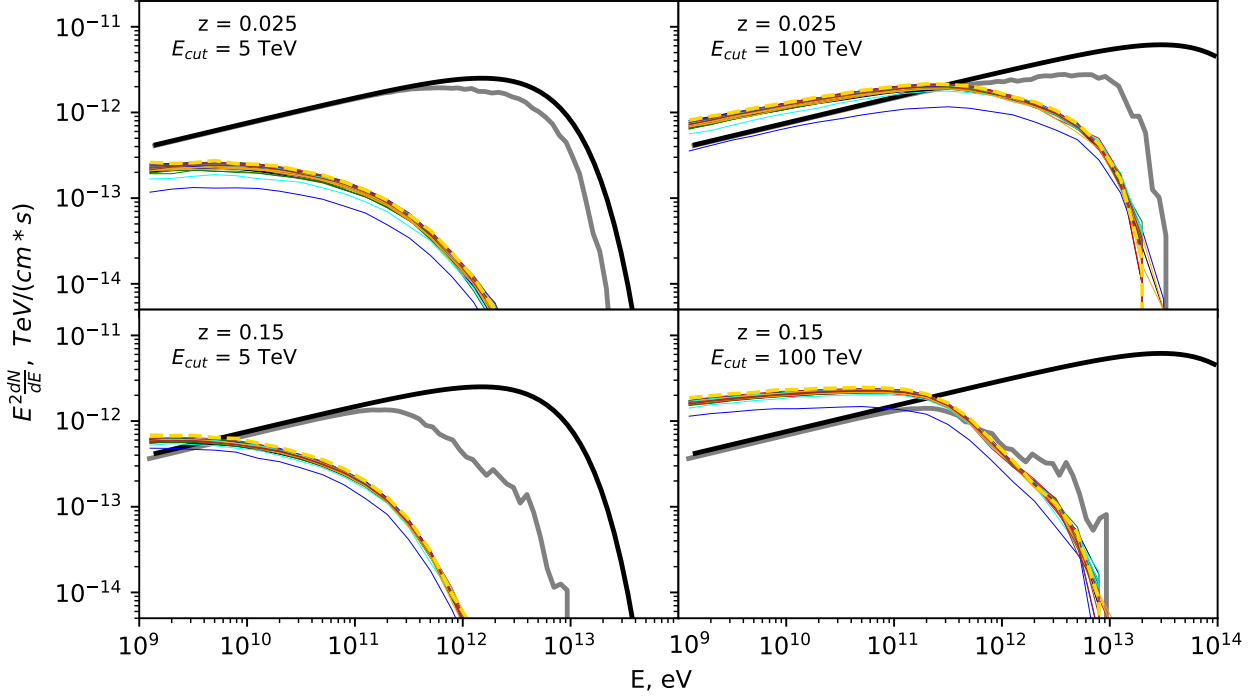


**Fig. 4.** Same as Fig. 3 but for the “only bubbles” magnetic field profiles (only regions with  $B < 10^{-12}$  G are taken into account). Colored solid lines indicate different lines of sight.

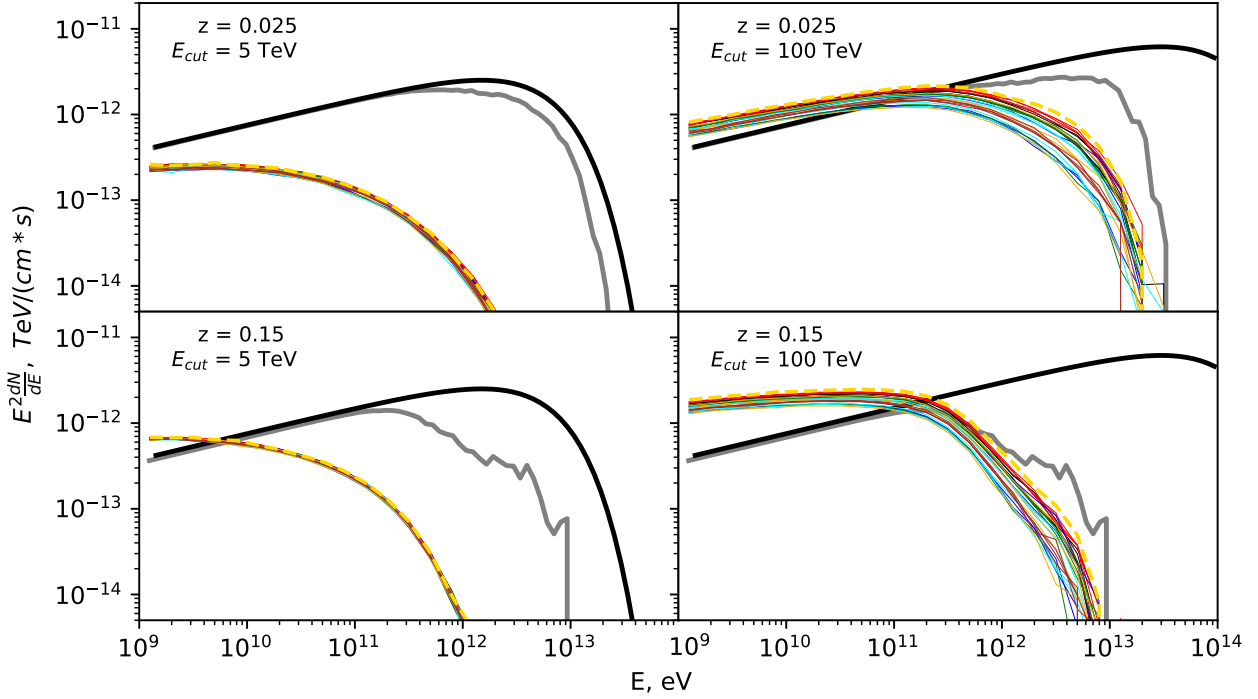


**Fig. 5.** Same as Figs. 3, 4 but for “only host bubble” magnetic field profile (only region with  $B > 10^{-12}$  G around the source galaxy is taken into account).

that within the TNG100 feedback model, the magnetized bubbles typically remove some 10% of the secondary  $\gamma$ -ray flux if the source intrinsic  $\gamma$ -ray spectrum has a high energy cut-off at relatively low energy  $E_{cut} \sim 5$  TeV. However, for a fraction of lines of sight, the pass of the photons through the initial bubble happens to be large (above 10 Mpc), and loss of the secondary emission for these cases is 2-3 times larger.

The average flux suppression gets stronger, up to 20%-50% for hypothetical sources with hard intrinsic spectra extending up to  $E_{cut} = 100$  TeV. Even though there is currently no observational evidence for the existence of such extreme AGN, we show the result for this case to highlight the dependence of the bubble effect on the intrinsic properties of the primary  $\gamma$ -ray source.

The secondary flux suppression by the bubbles is accumulated in the AGN host bubble and all other bubbles along the LOS. The relative importance of the “host” and “all other” bubbles also depends on the properties of the primary  $\gamma$ -ray source. This is illustrated in Fig. 6 which also shows the percentage of the lost secondary flux as a function of the bubble type.

The suppression by “all other” bubbles except for the AGN host bubble is at the level 5-20%, and it does not depend on either the distance to the source or the cut-off energy. In this case, the suppression factor is well described by the fraction of the LOS length occupied by the magnetized bubbles.

There is one singular LOS in Fig. 6 that happened to be affected by the bubbles much stronger (50-60%), despite a modest (5 Mpc) pass in the initial bubble. The reason for this phenomenon is clear from Fig. 2 – in this case, the LOS passes not only through the initial bubbles around the source but also through a large filamentary system of magnetized bubbles that occupy more than half of the first 100 Mpc of this line of sight. Although this seems to be a rare combination of the location of the source and the orientation of the LOS with respect to the filamentary system of bubbles, such a possibility can not be dismissed for any particular source (at least, according to the IllustrisTNG model).

The AGN host bubble has practically no effect on the secondary source flux if the cut-off energy  $E_{cut}$  is low. However, it has a strong impact on the signal from sources with high cut-off energy. In this case, the mean free path  $D_{mfp}(E_{cut})$  of the gamma-rays with energy  $E_{cut}$  becomes smaller than the size of the first bubble so that a significant fraction of primary  $\gamma$ -ray flux is absorbed inside this AGN host bubble. This significantly increases the percentage of lost secondary emission, as shown in Fig. 6. The effect is more substantial for higher cut-off energies, and it is slightly weakened for further away from sources due to additional contribution to the secondary flux from longer propagation to the observer. For the nearby source with high cut-off energy, additional losses in the first bubble can exceed 30%.

The range of the primary source parameters for which the losses in the first bubble are perceptible is shown in Fig. 7. Two source classes are clearly visible. Nearby sources with low cut-off energies are practically unaffected by the host AGN bubbles. This is true as long as the mean free path of gamma-rays  $D_{mfp}(E_{cut})$  is larger than the distance to the observer  $D_s$  so that the suppression factor is equal to the fraction of the LOS occupied by the bubble. This explains the “horizontal branch” of the contours in Fig. 7. As soon as the mean free path of the primary  $\gamma$ -rays gets shorter than the distance to the source, the fraction of the flux removed by the AGN host bubble is given by the ratio of the bubble size to the primary  $\gamma$ -ray mean free path  $D_{mfp}(E_{cut})$ . This effect is visible toward the higher energy “inclined” branch of the contours in Fig. 7. An important conclusion that can be drawn from Fig. 7. The presence of magnetized bubbles in the

LSS produces only a mild effect on the secondary  $\gamma$ -ray flux at 10% level for all reasonable AGN source parameters. In this respect, the bubbles have to be taken into account as an additional source of systematic uncertainties in the analysis of the IGMF in voids.

## 5. Discussion

The results presented above show that account of magnetic fields produced by the baryonic feedback on the LSS results in modifications of model calculations of the secondary  $\gamma$ -ray flux from electromagnetic cascade developing along the LOS. The strength of the effect depends on the parameters of the primary  $\gamma$ -ray source.

In the specific feedback model of IllustrisTNG, the effect is always at the level of  $\sim 10\%$  for a wide range of AGN primary source parameter choices: the cut-off energies below  $\sim 30$  TeV, redshifts within  $z \sim 0.15$ . In this case, the possible presence of magnetized bubbles along the LOS has to be considered as an additional source of systematic uncertainty of the overall level of the secondary flux. This systematic uncertainty does not affect the spectral shape of the secondary  $\gamma$ -ray flux. In general, it also does not affect the timing and extended emission profiles of the signal. This implies that previously developed analysis methods leading to constraints on the strength and correlation length of the void IGMF remain valid even in the presence of the magnetized bubbles.

It is interesting to note that the qualitative difference of the effect of the bubble and void IGMF on the  $\gamma$ -ray signal can be used to separate the two effects in the observational data. The bubbles completely randomize the directions of electrons and positrons in high magnetic field regions. In this respect, they produce the same effect independently of the energy of electrons and positrons. On the contrary, the void IGMF randomizes the directions of only low-energy electrons and positrons. If the primary source flux is well constrained (this suggests that high-statistics measurement of the attenuated point-source flux at the highest energy is available), the total secondary flux level can be reliably estimated. An overall energy-independent suppression of the secondary flux can therefore be measured. This can provide an estimate of the fraction of the line of sight occupied by the magnetized bubbles. The void IGMF is measurable through a different effect of the existence of extended or delayed emission below characteristic energy at which the IGMF is able to sufficiently deflect electrons and positrons away from the LOS.

The separation between the bubble and IGMF effects on the secondary  $\gamma$ -ray flux becomes less clear when the time delay of the cascade signal is very large or for sources with very high cut-off energy and hard intrinsic spectrum. In the first case, the intrinsic luminosity of the source cannot be constrained. In the last case, the mean free path of the primary  $\gamma$ -rays can be comparable to the size of the bubble around the AGN host galaxy. Suppression of the secondary flux can be large in this case (see Fig. 6). This introduces huge systematic uncertainty to the model of the secondary  $\gamma$ -ray flux. This uncertainty can preclude the possibility of the estimate of IGMF, especially if the statistics of the  $\gamma$ -ray data on the extended or delayed signal is poor.

## 6. Conclusions

In this paper, we have explored the effect of the baryonic feedback on the LSS in the form of outflows from galaxies that “pollute” the intergalactic medium with magnetic fields. This process can spread the magnetic field in the voids of the LSS and

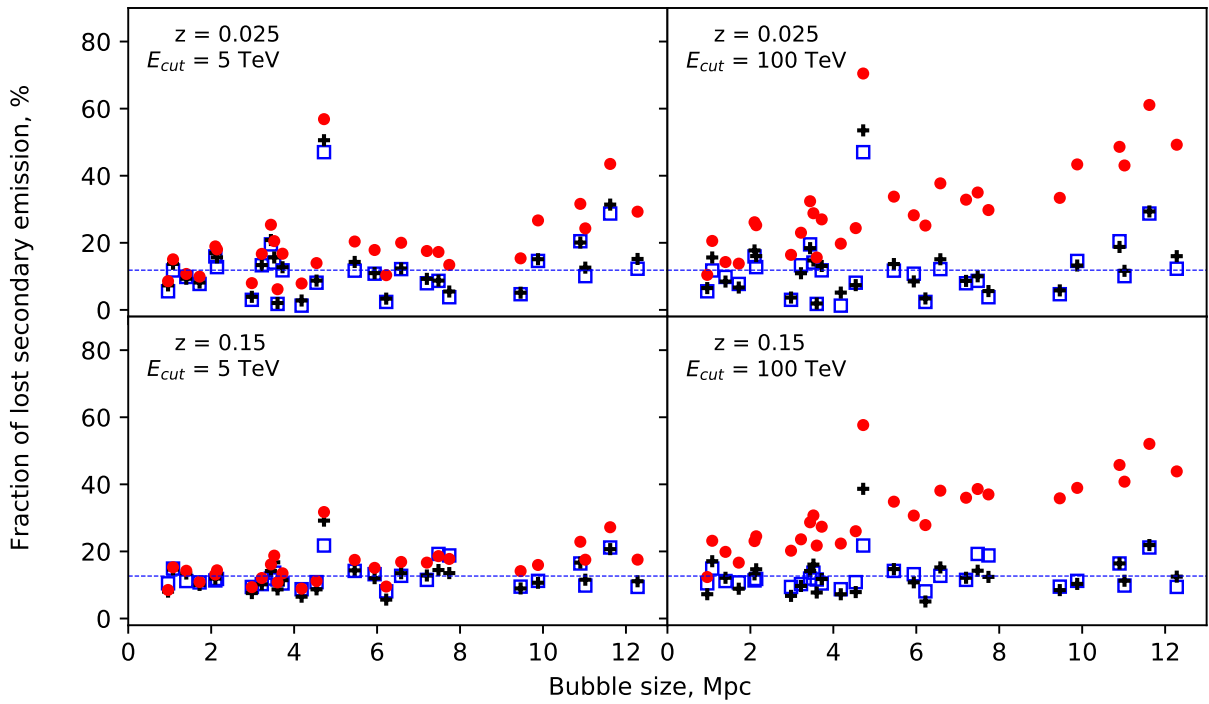


**Fig. 6.** Fraction of the secondary  $\gamma$ -ray flux in the energy range 1-10 GeV removed by the bubbles, as a function of the size of the host AGN bubble. Red circles show the flux fractions removed by all bubbles. Black crosses and blue squares show the flux fractions removed by all bubbles except for the host AGN bubble and a linear fraction of the line of sight occupied by these bubbles. Blue dashed horizontal line marks the average linear fraction of the line of sight occupied by all bubbles except for the host AGN bubble.

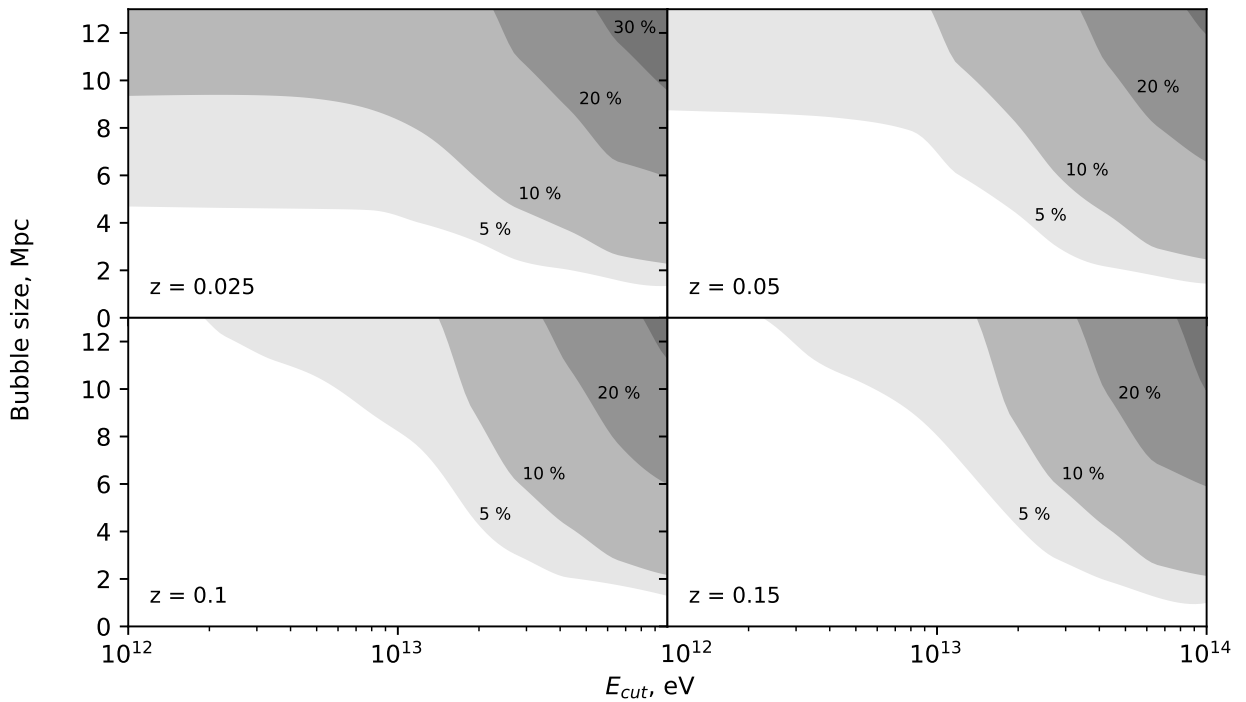


**Fig. 7.** Fraction of the secondary flux in the energy range 1-10 GeV removed by the host AGN bubble as a function of cutoff energy and size of the bubble.

thus preclude the possibility of measurement of primordial magnetic fields that possibly reside in the voids.

Our analysis of the specific baryonic feedback model implemented in IllustrisTNG cosmological simulations shows that the feedback generally does not strongly affect the void magnetic fields. The galactic outflows from magnetized bubbles collectively have a small volume filling factor.

We have explored the effect of the magnetized bubbles on the  $\gamma$ -ray signal from distant AGN. This  $\gamma$ -ray signal is used for the measurements of magnetic fields in the voids. We have characterized the influence of the magnetized bubbles on the signal and found that they typically produce an overall suppression of the secondary flux. Within the IllustrisTNG baryonic feedback model, the effect is generally small, at the level of  $\sim 10\%$  for representative parameters of the primary AGN  $\gamma$ -ray sources. However, we have found in our sample one line of sight for which effect is of order 60% because of massive pollution of the first 100 Mpc by magnetic bubbles. Therefore, working with a single source, one can never exclude such a possibility. Robust measurements have to rely on a large sample of sources. In this case, the effect of magnetized bubbles on the  $\gamma$ -ray signal (energy-independent suppression of secondary flux) is readily distinguishable from the effect of the void magnetic fields (that completely suppresses the secondary  $\gamma$ -ray flux below some characteristic energy).

The effect of outflow-driven magnetized bubbles can be taken into account in the analysis as a systematic uncertainty of the secondary  $\gamma$ -ray flux, at the level of 10% in average (and up to 60% for a single source). This error has to be taken in the error budget of the analysis. This systematic uncertainty depends on the high energy cut-off of the primary source spectrum. If the cut-off energy in  $E_{\text{cut}} = 100$  TeV range, dedicated analysis of possible properties of the AGN host bubble have to be assessed as part of the IGMF-related data analysis.

## 7. ACKNOWLEDGEMENTS

Work of D.S. and A.N. has been supported in part by the French National Research Agency (ANR) grant ANR-19-CE31-0020, work of A.K. was supported in part by Russian Science Foundation grant 20-42-09010. A.K.'s stay in the APC laboratory was provided by the ‘‘Vernadsky’’ scholarship of the French embassy in Russia. K.B. and A.B. are supported by the European Research Council (ERC) Advanced Grant ‘‘NuBSM’’ (694896). A.S. is supported by the FWF Research Group grant FG1.

## References

- Abdalla, H. et al. 2021, JCAP, 02, 048  
 Ackermann, M. et al. 2018, *Astrophys. J. Suppl.*, 237, 32  
 Benitez-Llambay, A. 2015, py-sphviewer: Py-SPHViewer v1.0.0  
 Berezhinsky, V. & Kalashev, O. 2016, *Phys. Rev. D*, 94, 023007  
 Bertone, S., Vogt, C., & Ensslin, T. 2006, *Mon. Not. Roy. Astron. Soc.*, 370, 319  
 Dermer, C. D., Cavadini, M., Razzaque, S., et al. 2011, *ApJ*, 733, L21  
 Dolag, K., Kachelriess, M., Ostapchenko, S., & Tomas, R. 2011, *Astrophys. J. Lett.*, 727, L4  
 Durrer, R. & Neronov, A. 2013, *Astron. Astrophys. Rev.*, 21, 62  
 Garcia, A. A., Bondarenko, K., Boyarsky, A., et al. 2020 [arXiv:2011.11581]  
 Garcia, A. A., Bondarenko, K., Boyarsky, A., et al. 2021 [arXiv:2101.07207]  
 Gilmore, R. C., Somerville, R. S., Primack, J. R., & Dominguez, A. 2012, *Mon. Not. Roy. Astron. Soc.*, 422, 3189  
 Kachelriess, M., Ostapchenko, S., & Tomas, R. 2012, *Comput. Phys. Commun.*, 183, 1036  
 Kalashev, O. & Kido, E. 2015, *J. Exp. Theor. Phys.*, 120, 790  
 Korochkin, A., Kalashev, O., Neronov, A., & Semikoz, D. 2021, *Astrophys. J.*, 906, 116  
 Marinacci, F., Vogelsberger, M., Pakmor, R., et al. 2018, *MNRAS*, 480, 5113

- Naiman, J. P., Pillepich, A., Springel, V., et al. 2018, *MNRAS*, 477, 1206  
 Nelson, D., Pillepich, A., Springel, V., et al. 2019a, *MNRAS*, 490, 3234  
 Nelson, D., Pillepich, A., Springel, V., et al. 2018, *MNRAS*, 475, 624  
 Nelson, D., Springel, V., Pillepich, A., et al. 2019b, *Computational Astrophysics and Cosmology*, 6, 2  
 Neronov, A. & Semikoz, D. 2009, *Phys. Rev. D*, 80, 123012  
 Neronov, A. & Semikoz, D. V. 2007, *JETP Lett.*, 85, 473  
 Neronov, A. & Vovk, I. 2010, *Science*, 328, 73  
 Pakmor, R., Bauer, A., & Springel, V. 2011, *MNRAS*, 418, 1392  
 Pakmor, R. & Springel, V. 2013, *MNRAS*, 432, 176  
 Pillepich, A., Nelson, D., Hernquist, L., et al. 2018a, *MNRAS*, 475, 648  
 Pillepich, A., Springel, V., Nelson, D., et al. 2018b, *MNRAS*, 473, 4077  
 Pinsonneault, S., Martel, H., & Pieri, M. M. 2010, *Astrophys. J.*, 725, 2087  
 Plaga, R. 1995, *Nature*, 374, 430  
 Planck Collaboration, Ade, P. A. R., et al. 2016, *A&A*, 594, A13  
 Springel, V. 2010, *MNRAS*, 401, 791  
 Springel, V., Pakmor, R., Pillepich, A., et al. 2018, *MNRAS*, 475, 676  
 Taylor, A., Vovk, I., & Neronov, A. 2011, *Astron. Astrophys.*, 529, A144  
 Weinberger, R., Springel, V., Hernquist, L., et al. 2017a, *MNRAS*, 465, 3291  
 Weinberger, R., Springel, V., Hernquist, L., et al. 2017b, *MNRAS*, 465, 3291